Spatial Distribution of Magnetic Reconnection in the 2006 December 13 Solar Flare As Observed by Hinode

Ju Jing[1,2], Jongchul Chae[3], and Haimin Wang[1,2]

1. Center for Solar-Terrestrial Research, New Jersey Institute of Technology, Newark, NJ 07102

2. Big Bear Solar Observatory, 40386 North Shore Lane, Big Bear City, CA 92314

3. Astronmy Program, Department of Physics and Astronomy, Seoul National University, Seoul, 151-742, Korea

ABSTRACT

A massive two-ribbon flare and its source magnetic field region were well captured by Solar Optical Telescope (SOT) on board *Hinode* in Ca II H spectral line and by Spectro-Polarimeter (SP) of SOT, respectively. Using the high resolution *Hinode* data sets, we compare the spatial distribution of local magnetic reconnection rate and energy release rate along the ribbons with that of G-band kernels which serve as a proxy for the primary energy release. The G-band kernels spatially coincide with the maximum of both modelled quantities, which gives strong support for the reconnection model. We also investigate the magnitude scaling correlation between the ribbon separation speed V_r and magnetic field strength B_n at four 2-min time bins around the maximum phase of the flare. It is found that V_r is weakly and negatively correlated with B_n. An empirical relation of $V_r \propto B_n^{-0.15}$ is obtained at the flare peak time with an correlation coefficient $\sim$ -0.33. The correlation is weaker at other time bins.

Subject headings: Sun: activity — Sun: magnetic fields — Sun: flares

1. INTRODUCTION

Separating flare ribbons are regarded as the most solid evidence for the standard magnetic reconnection scenario (known as the CHSKP model; Carmichael 1964; Sturrock 1966; Hirayama 1974; Kopp & Pneuman 1976), and serve as the mapping of the coronal magnetic reconnection onto the visible surface. Under the principle of magnetic flux conservation, Forbes & Priest (1984) supplemented the CSHKP model for a quantitative estimate of the coronal magnetic

reconnection rate in the reconnecting current sheet (RCS) from observable quantities, i.e., $\varphi_{rec} = \int V_r B_n \, dl = \frac{\partial}{\partial t} \int B_n \, da$, where V_r is the ribbon separation velocity, B_n is the normal component of the local magnetic field strength measured in the ribbon location, dl is the length along the ribbons and da is the newly brightened area swept by the ribbons. In particular, $E = V_r B_n$ is the electric field at the reconnecting X-point and often used as a local magnetic reconnection rate. In the meanwhile, the magnetic energy release rate derived from Poynting vector theorem is proportional to $V_r B_n^2$ under the common assumption that B_c/B_n and A_c are constant during the flare (Isobe et al. 2002), in which B_c is the strength of coronal field line coming into the X-point and A_c is the area of the RCS. Since then, as a test of the model, temporal and spatial correlations of these modelled quantities with observed flare nonthermal emissions (e.g., hard X-rays, microwaves) have been investigated in many studies, and are found to be good in most cases of temporal comparison (e.g., Qiu et al. 2004; Asai. 2004; Jing et al. 2005; Lee et al. 2006; Miklenic et al. 2007).

On the other hand, the spatial distribution of these quantities as a function of ribbon position is a hard issue involving the complexity of coronal magnetic field. A theoretical framework of CSHKP model only deals with two-dimensional (2D) configuration with a translational symmetry along the reconnecting X-line (the third dimension). From an observational point of view, however, almost all spatial properties of the ribbon motion and magnetic structure addressed in recent works apparently lack such translational symmetry (e.g., Fletcher et al. 2004; Grigis & Benz 2005; Temmer et al. 2007). For instance, the inhomogeneity of magnetic field and energy release rate along the flare ribbons was first addressed by Asai et al. (2002) and recently by Temmer et al. (2007). Both of them found that the magnitude difference is up to a factor of 3 in the case of magnetic field and about 2 orders for the energy release rate along the ribbons. The ribbon sections with the strongest magnetic field strength and energy release rate spatially coincide with the site of hard X-ray (HXR) footpoint sources which serve as a proxy for the primary energy release. Jing et al. (2007) extended the work by measuring the intensity distribution of a ribbon-like HXR source that has been rarely observed before. In their result, the HXR evolved from footpoint to ribbon-like sources and the spatial correlation between the HXR intensity and the electric field decreased. In an effort to provide an insight into another aspect of the model, Xie et al. (2007) performed a detailed analysis of the V_r-B_n relationship during a well-observed two-ribbon flare at selected times and found a weak dependence of $V_r \propto B_n^{-0.18}$ at the time of flare maximum. All these studies concern the structure along the ribbon that is not directly described by the 2D model.

With the launch of the *Hinode* spacecraft (formerly known as *Solar-B*; Kosugi et al. 2007), flares have been observed at unprecedented spatial resolution. The magnetic field strength of source regions, specially in the strong magnetic regions, have been measured with higher accuracy as Zeeman saturation effect is significantly reduced. In this Letter we revisit the issue

of the spatial distribution of the modelled quantities along the ribbons during a massive flare of 2006 December 13, with *Hinode* data sets and with our new techniques of image processing. We also examine the magnitude scaling correlation between the ribbon separation velocity and magnetic field strength.

2. Data Sets and Imaging Processing

The 4B/X3.4 flare we discuss in this Letter occurred in active region NOAA 10930 on 2006 December 13 and was captured by Solar Optical Telescope (SOT; Tsuneta et al. 2007) on board *Hinode*. The Broadband Filter Imager (BFI) of SOT obtained data in Ca II H spectral line (397 nm) and G-band (430 nm) with a 2 min cadence and a pixel size of 0.108". Spectro-Polarimeter (SP) of SOT obtained Stokes profiles (I, Q, U and V) of two magnetically sensitive Fe lines at 630.15 nm and 630.25 nm. The line-of-sight magnetogram was determined from Stokes I and V profiles using the Center-of-Gravity method. Compared with previous line-of-sight magnetogram data, *Hinode* magnetogram data have advantages in higher spatial resolution and more accurate field strength measurements without saturation effect.

We need to trace multiple locations within a ribbon as it moves out. Once these points are located at each time, the velocity V_r can be derived as a function of time and/or distance along the ribbon. For this purpose, we have developed a method involving Sobel edge detection algorithm, Otsu Thresholding algorithm (Otsu 1979) and some morphology processing techniques (Qu et al. 2004) to extract the outer edges of the ribbons. In particular, we first apply Sobel edge detector to the Ca II H images to enhance the edges. Then we apply Otsu thresholding algorithm to automatically find the threshold that can separate the edges from the background with the maximum between-class variance. The edges determined so far include both outer edges and inner edges of the ribbons and only the former is of interest in this study. Therefore, we scan each pair of edges along the direction perpendicular to the magnetic polarity inversion lines (PILs). An edge is defined as being an outer edge if it has a longer distance to PILs compared to its counterpart. Finally, we use morphology closing to eliminate small gaps between feature regions. Figure 1 shows the outer edges of the ribbons detected with our method, superposed on a *Hinode* line-of-sight magnetogram.

3. Results

The top panel of Figure 2 is a Ca II H line image taken at the time of the flare maximum, 02:28 UT. The middle panel shows the co-aligned line-of-sight magnetogram overlaid with

the magnetic PILs (black curves). The alignment between SOT-Ca II and SOT-SP images is performed by manually aligning the spots and network structures. The blue and yellow lines show the outer edges of the ribbons obtained at 02:28 UT and 02:30 UT, respectively. j_1 (running from 0 to 150) and j_2 (running from 0 to 50) are the index of the multiple points which are evenly spaced along two edges. The dotted boxes are drawn to mark the field-of-view of the G-band images presented in the bottom three panels.

As mentioned in §1, the 2D reconnection model (Forbes & Priest 1984) predict that the magnetic reconnection rate is given by $V_r B_n$ and the energy release rate is proportional to $V_r B_n^2$. We note that ribbons in this case are moving rather nonuniformly and the motion in weak magnetic field seems to be more complex. It implies the complex magnetic configuration in weak magnetic field regions that may not be explained with the simple 2D reconnection model. Therefore, this study only focus on the parts of the ribbons on the strong magnetic field ($j_1 = 50 - 115$ and $j_2 = 0 - 50$). Determination of B_n is straightforward–we can just read from the co-registered magnetogram, but it is hard to determine the velocity distribution along the ribbon, since we have no obvious tracers within the ribbon. To simplify the calculation, we use the index j as the motion tracer, measure the displacements of points, and divide them by the time interval. We then apply the cosine of the relative angle to the magnetic PILs to finally take only the velocity components perpendicular to the PILs as V_r. The accuracy of the velocity derived in this way is limited by our assumption that the points along the outer edge can be properly traced by their relative locations along the edge. This assumption may not be valid in general, but should not seriously affect the velocity presented in this study because of the nature of curent observation. We estimate the uncertainty by manually tracking serval noticeable features taken as reference points and comparing them with the result derived in this way. The uncertainty is estimated to be less than 20%.

We need to compare the magnetic reconnection rate $V_r B_n$ and energy release rate $V_r B_n^2$ with the energy deposition as observed with HXR for agreement. However, the HXR observation of this event at this time is not available. In this case, we take G-band kernels seen in the G-band difference image instead, because these kernels are also attributed to non-thermal flare emissions (Xu et al. 2004). The left two panels in the bottom of Figure 2 are two G-band images taken before and during the flare. In their difference image (rightmost), two ribbon kernels at either side of PILs are enhanced in white and indicated by the arrows.

In Figure 3 we plot the intensity profiles of B_n, V_r, $V_r B_n$ and $V_r B_n^2$ along the coordinate index j_1 and j_2 for two ribbons. The G-band kernels within two ribbons appear in the confined regions that are marked by the grey bars. We note that both B_n and V_r show a certain degree of inhomogeneity along the ribbons. As a result, $V_r B_n$ and $V_r B_n^2$ are not uniform along the ribbons. The peaks of B_n, $V_r B_n$ and $V_r B_n^2$ spatially coincide with the sites of G-band kernels.

Such a spatial correlation supports the conventional idea that magnetic reconnection can be, while occurring everywhere along the X-line, locally enhanced in the regions with strong field strength. The average $V_r B_n$ of $\sim$ 20 V cm^{-1} within the G-band kernel regions is larger, by a factor of approximately 2.5, than that in the regions off from the G-band kernels. In previous studies, the values of $V_r B_n$ are mostly in the range of 0.2-5 V cm^{-1}, up to $\sim$ 40 V cm^{-1} in the case of the exetremely dramatic flare on 2003 October 29 (Jing et al. 2005).

Both V_r and B_n are contributing factors in deriving the magnetic reconnection rate and energy release rate. We further investigate V_r-B_n relationship. Since the actual length and morphology of the ribbon keep varying with time as the ribbon evolves, we only choose four 2-min time intervals ($a - d$) from 02:24 UT to 02:32 UT around the peak time of the flare, divide the outer edges into many small sections ($\sim$15 for the northern ribbon and $\sim$10 for the southern ribbon) and trace them individually. Then we calculated the average velocity and average field strength of each corresponding section. Figure 4 shows the scatter plots of V_r vs. B_n in a logarithmic scale for four time intervals. It is notable that V_r is weakly and negatively correlated with B_n. The correlation coefficients, from (a) to (d), are -0.29, -0.16, -0.33 and -0.04, respectively. The solid line is a fit to the data points in a form of (a): $V_r = 85.1 \times B_n^{-0.27}$; (b): $V_r = 38.9 \times B_n^{-0.12}$; (c): $V_r = 29.3 \times B_n^{-0.15}$; and (d): $V_r = 10.5 \times B_n^{-0.03}$. The relation at the flare peak time (c) is very similar to another empirical relation of $V_r = 34.2 \times B_n^{-0.18}$ obtained during the X2.3 flare of 2001 April 10 (Xie et al. 2007).

4. Summary

The standard magnetic reconnection model allows quantitative estimate of the magnetic reconnection rate and magnetic energy release rate from flare observation. Since the observation of the locally confined G-band kernels is another proxy for the primary energy release, comparison of these quantities with G-band kernels in space can serve as a test of the model. With the high-resolution *Hinode* data set and our new techniques of image processing, we revisited the issue of spatial distribution of magnetic field B_n and two modelled quantities, $V_r B_n$ and $V_r B_n^2$. The former is equivalent to the coronal electric field (a simplified magnetic reconnection rate), while the latter is a proxy for the energy release rate under the assumption that B_c/B_n and A_c do not vary with time.

It is found that there is a certain degree of inhomogeneity in these quantities along the ribbons, indicating the inhomogeneity in the coronal magnetic reconnection. We can see a good agreement between the sites of G-band kernels and the strongest magnetic field regions. The average B_n within the G-band kernel regions is $\sim$ 2 times larger than that in the non-kernel regions, which comparable with the previous observation by Asai et al. (2002). In the presence

of such a magnetic field inhomogeneity along the ribbons, the maximum reconnection rate and the maximum energy release rate appear in G-band kernel regions as well.

The average $V_r B_n$ found in G-band kernel regions, ~ 20 V cm^{-1}, is larger than the typical range of $0.2 - 5$ V cm^{-1} reported in previous studies of flares that were not accompanied by the G-band emissions, but less than ~ 40 V cm^{-1} derived in the 2003 October 29 flare. The 2003 October 29 flare is also known as the first white-light flare observed in the near-infrared (NIR) continuum at 1560 nm, the deepest photospheric layer. As Xu et al. (2004) pointed out, "back-warming" mechanism may be responsible for the enhanced NIR emission. Though the G-band is not directly heated by precipitating electrons, the backwarming process depends on the energy carried by nonthermal electrons. So G-band emission is considered as an indirect diagnosis of nonthermal electrons. It is thus conceivable that $V_r B_n$ derived from the local flare observations indeed provide a clue to the initial energy of electrons obtained in the acceleration process during the magnetic reconnection in the RCS. We further presume that a few tens of electric field strength in V cm^{-1} might be a crucial threshold to generate white-light part of a flare.

We also examined V_r-B_n relationship on the relatively strong magnetic field ($B_n > 200$ Gauss) and found a weak, negative correlation between the quantities. An empirical relation of $V_r \propto B_n^{-0.15}$ at the flare peak time was found in this case. This is very similar to another empirical relation of $V_r \propto B_n^{-0.18}$ obtained during the X2.3 flare of 2001 April 10 (Xie et al. 2007). Our empirical relation accordingly suggests that magnetic reconnection rate and energy release rate are proportional to $B_n^{0.85}$ and $B_n^{1.85}$, respectively. For instance, spatial variation of field strength by a factor of 2 may lead to a contrast by a factor of $\sim$1.8 in the magnetic reconnection rate and $\sim$3.6 in the energy release rate. It explains why the high energy release regions (e.g., HXR sources, G-band kernels) tend to be concentrated to local strong field regions.

The authors are grateful for Jeongwoo Lee for helpful discussions. The authors thank *Hinode* and team for excellent data set. *Hinode* is a Japanese mission developed and launched by ISAS/JAXA, collaborating with NAOJ as a domestic partner, NASA and STFC (UK) as international partners. Scientific operation of the Hinode mission is conducted by the Hinode science team organized at ISAS/JAXA. This team mainly consists of scientists from institutes in the partner countries. Support for the post-launch operation is provided by JAXA and NAOJ (Japan), STFC (U.K.), NASA, ESA, and NSC (Norway). JJ, and HW were supported by NSF under grant ATM-0716950, ATM-0548952 and NASA under grant NNX0-7AH78G. JC was supported by the Korea Research Foundation Grant funded by the Korean Government (KRF-2005-070-C00059)

REFERENCES

Asai, A., Masuda, S., Yokoyama, T., Shimojo, M., Isobe, H., Kurokawa, H., & Shibata, K., 2002, ApJ, 578, L91

Asai, A., Yokoyama, T., Shimojo, M., Masuda, S., Kurokawa, H., & Shibata, K., 2004, ApJ, 611, 557

Carmichael, H., 1964, in The Physics of Solar Flares, ed. W. N. Hess (NASA SP-50; Washington, DC:NASA), 451

Fletcher, L., Pollock, J. A., & Potts, H. E. 2004, Sol. Phys., 222, 279

Forbes, T.G. & Priest, E.R.: 1984, in Solar Terrestrial Physics: Present and Future, ed. D.M. Butler, K. Papadopoulous (NASA RP-1120, Washington, D.C.) p 1

Grigis, P. C., & Benz, A. O., 2005, ApJ, 625, 143

Hirayama, T., 1974, Sol. Phys., 187, 229

Isobe, H., Yokoyama, T., Shimojo, M., Morimoto, T., Kozu, H., Eto, S., Narukage, N., & Shibata, K., 2002, ApJ, 566, 528

Jing, J., Qiu, J., Lin, J., Qu, M., Xu, Y., & Wang, H., 2005, ApJ, 620, 1085

Jing, J., Lee, J., Liu, C., Gary, D. E., Wang, H., 2007, ApJ, 664, L127

Kopp, R. A., & Pneuman, G. W., 1976, Sol. Phys., 50, 85

Kosugi, T., Matsuzaki, K., Sakao, T., Shimizu, T., Sone, Y., Tachikawa, S., Hashimoto, T., Minesugi, K., Ohnishi, A., Yamada, T., Tsuneta, S., Hara, H., Ichimoto, K., Suematsu, Y., Shimojo, M., Watanabe, T., Davis, J.M., Hill, L.D., Owens, J.K., Title, A.M., Culhane, J.L., Harra, L., Doschek, G.A., & Golub, L., 2007, Sol. Phys., in press

Lee, J., Gary, D. E., & Choe, G. S., 2006, ApJ, 647, 638

Miklenic, C. H., Veronig, A. M., Vršnak, B., & Hanslmeier, A., 2007, A&A, 461, 697

Otsu, N.: 1979, IEEE Trans.Syst.Man. Cyber.SMC, 9(1), 62.

Qiu, J., Wang, H., Cheng, C. Z., & Gary, D. E., 2004, ApJ, 604, 900

Qu, M., Shih, F., Jing, J., & Wang, H., 2004, Sol. Phys., 222, 137

Sturrock, P. A. 1966, Nature, 211, 695

Temmer, M., Veronig, A. M., Vršnak, B., & Miklenic, C., 2007, ApJ, 654, 674

Tsuneta, S., Suematsu, Y., Ichimoto, K., Shimizu, T., Otsubo, M., Nagata, S., Katsukawa, Y., Title, A., Tarbell, T., Shine, R., Rosenberg, B., Hoffmann, C., Jurcevich, B., Levay, M., Lites, B., Elmore, D., Matsushita, T., Kawaguchi, N., Mikami, I., Shimada, S., Hill, L., & Owens, J., 2007, Sol. Phys., submitted

Xie, W., Zhang, H., & Wang, H., 2007, ApJ, submitted

Xu, Y., Cao. W., Liu, C., Yang, G., Qiu, J., Jing, J., Denker C., & Wang, H., 2004, ApJ, 131, 134

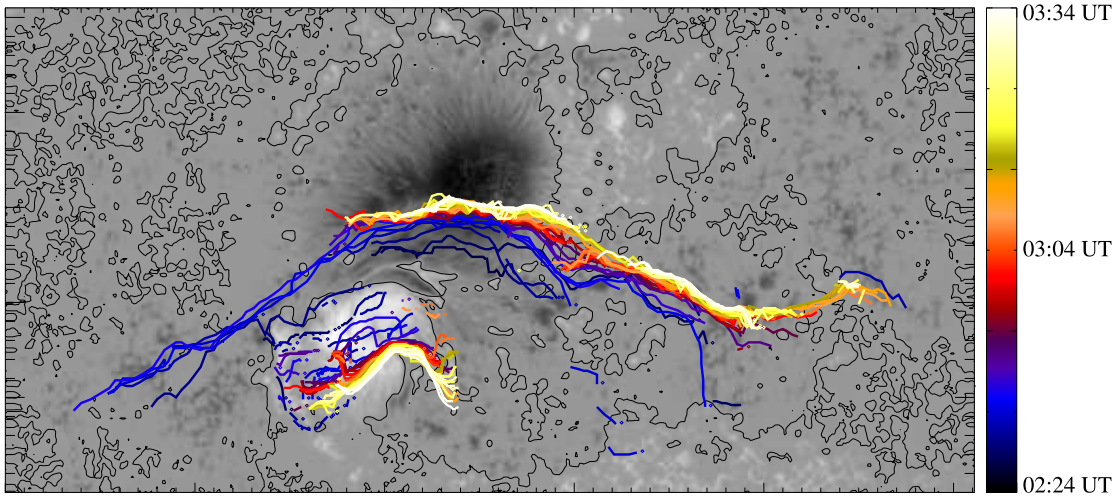

Fig. 1.— The detected outer edges of the flare. The background image is *Hinode* line-of-sight magnetogram. The field of view is 216" by 108".

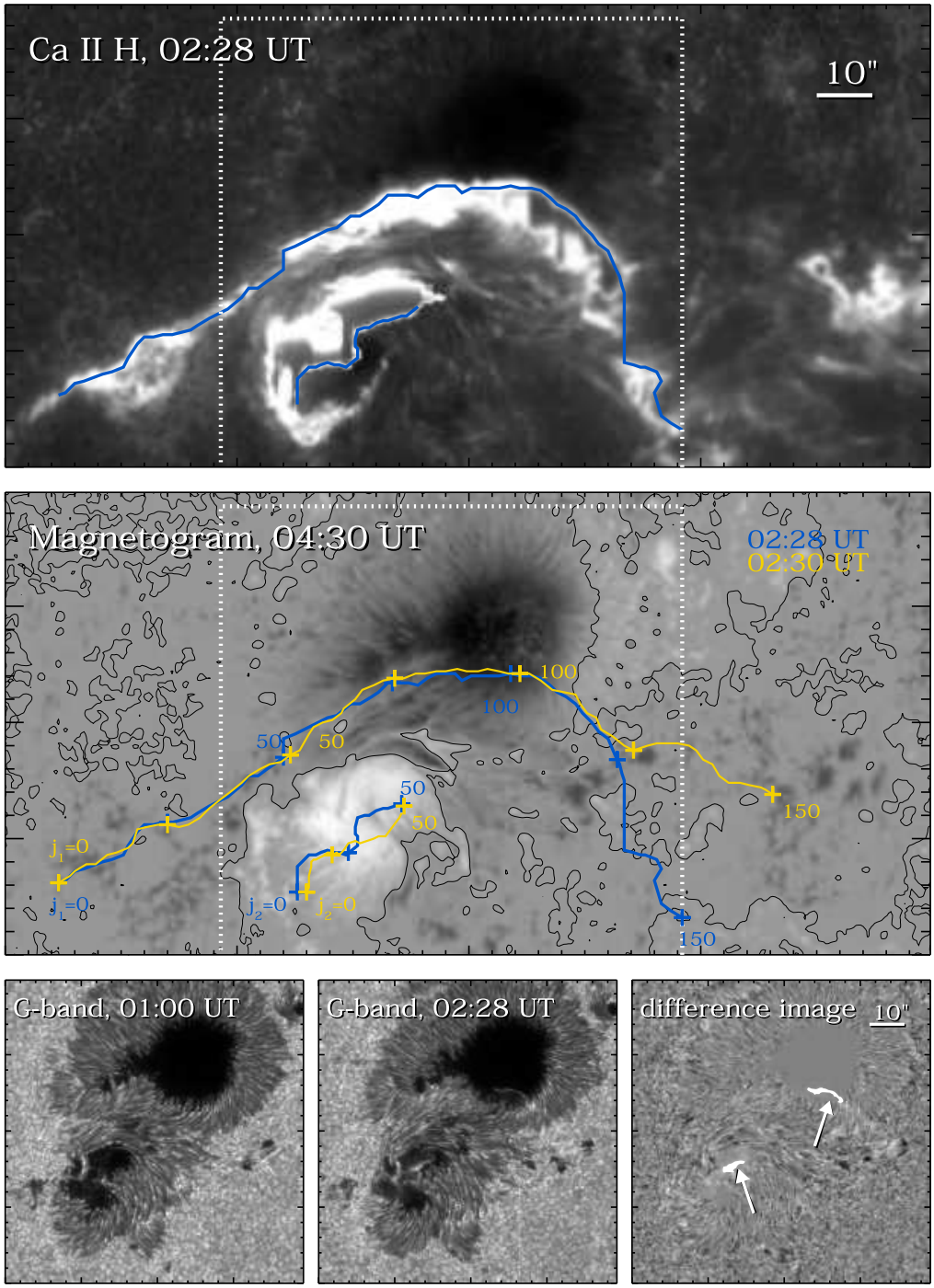

Fig. 2.— Top: Snapshot of the X3.4 flare observed by *Hinode* in CaII H line. Middle: *Hinode* line-of-sight magnetogram. Bottom: from left to right, *Hinode* G-band images taken before and after the flare, and their difference image. The symbol connected lines show locations of outer edges of ribbons. The dotted boxes show the field-of-view of the G-band images presented in the bottom three panels. The G-band kernels enhanced in white are indicated by the arrows.

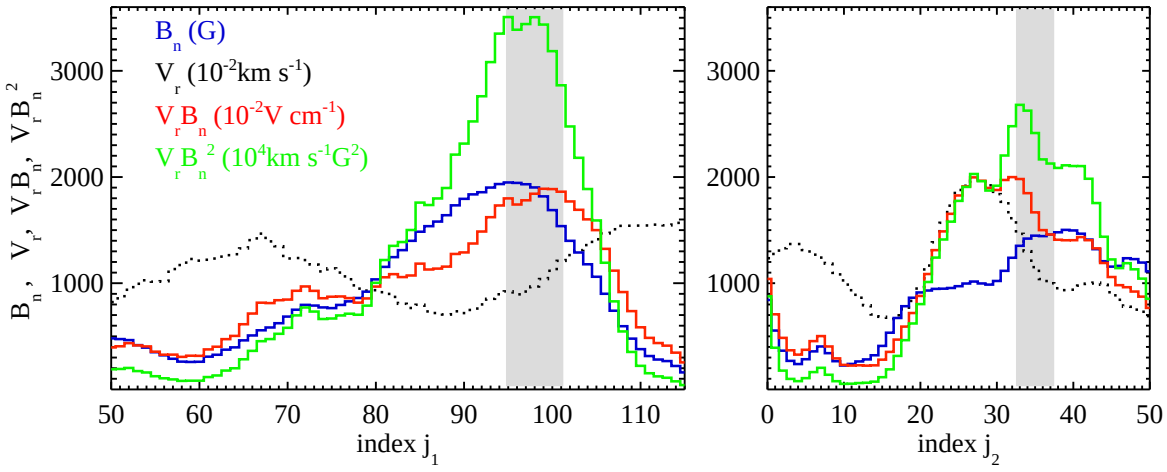

Fig. 3.— The spatial distribution of B_n (blue), V_r (grey dots), $V_r B_n$ (red) and $V_r B_n^2$ (green) along the index $j_1 = 50 - 115$ (left panel) and $j_2 = 0 - 50$ (right panel). The grey bars indicate the locations of two G-band kernels in accordance with the j_1 and j_2

.

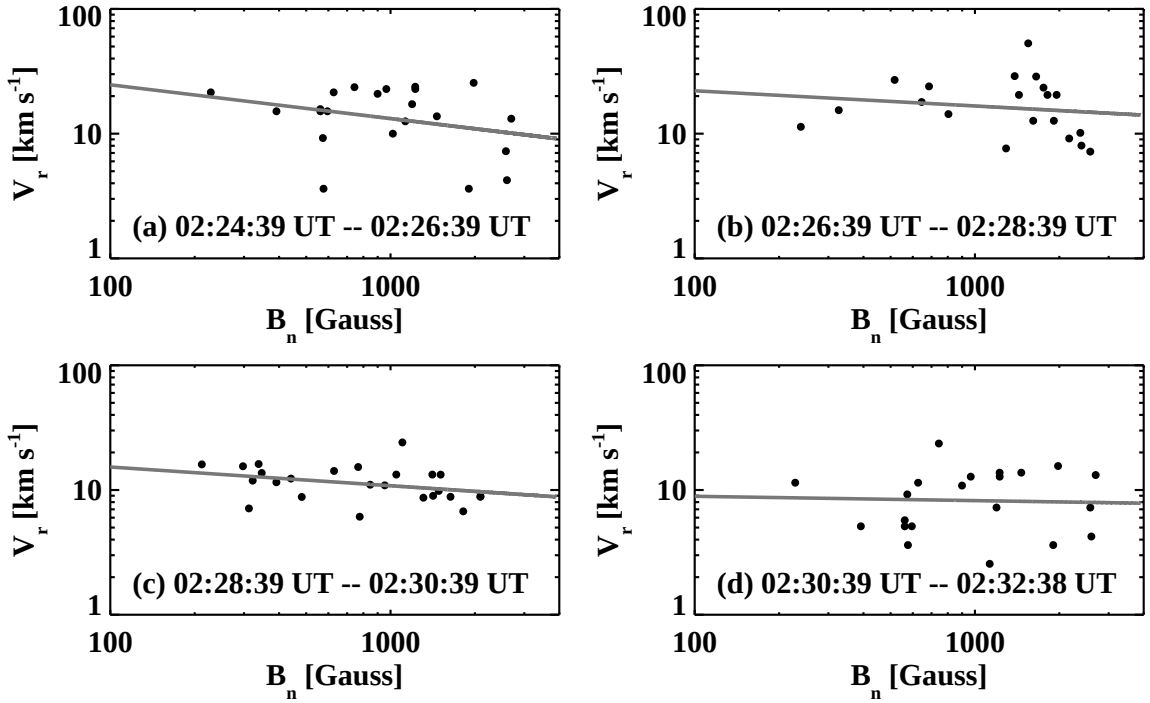

Fig. 4.— Scatter plots of V_r vs. B_n in a logarithmic scale for four time intervals (a)-(d). V_r and B_n refer to the average value of small ribbon sections at four time intervals. The solid line is a fit to the data points in the form of (a): $V_r = 85.1 \times B_n^{-0.27}$; (b): $V_r = 38.9 \times B_n^{-0.12}$; (c): $V_r = 30.2 \times B_n^{-0.15}$; and (d): $V_r = 10.5 \times B_n^{-0.03}$. The correlation coefficients, from (a) to (d), are -0.29, -0.16, -0.33 and -0.04, respectively.